Kobe University Repository : Kernel

PDF issue: 2025-07-11

Hybrid Rubisco with Complete Replacement of Rice Rubisco Small Subunits by Sorghum Counterparts Confers C4 Plant-like High Catalytic Activity

Matsumura, Hiroyoshi ; Shiomi, Keita ; Yamamoto, Akito ; Taketani, Yuri ; Kobayashi, Noriyuki ; Yoshizawa, Takuya ; Tanaka, Shun-ichi ;…

(Citation)
Molecular Plant,13(11):1570-1581

(Issue Date)
2020-11-02

(Resource Type)
journal article

(Version)
Accepted Manuscript

(Rights)
© The Author 2020.
This manuscript version is made available under the CC-BY-NC-ND 4.0 license
http://creativecommons.org/licenses/by-nc-nd/4.0/

(URL)
https://hdl.handle.net/20.500.14094/90007637

KOBE UNIVERSITY

Hybrid Rubisco with Complete Replacement of Rice Rubisco Small Subunits by Sorghum Counterparts Confers C_4-Plant-like High Catalytic Activity

Hiroyoshi Matsumura,[1,*] Keita Shiomi,[2] Akito Yamamoto,[2] Yuri Taketani,[3] Noriyuki Kobayashi,[2] Takuya Yoshizawa,[1] Shun-ichi Tanaka,[1,5] Hiroki Yoshikawa,[1] Masaki Endo,[4] Hiroshi Fukayama,[2,6,*]

[1]Department of Biotechnology, College of Life Sciences, Ritsumeikan University, 1-1-1 Noji-Higashi, Kusatsu 525-8577, Japan
[2]Graduate School of Agricultural Science, Kobe University, 1-1 Rokkodai-tyou, Nada-ku, Kobe 657-8501, Japan
[3]Faculty of Agriculture, Kobe University, 1-1 Rokkodai-tyou, Nada-ku, Kobe 657-8501, Japan
[4]Division of Applied Genetics, Institute of Agrobiological Sciences, National Agriculture and Food Research Organization, 1-2 Owashi, Tsukuba 305-8634, Japan
[5]Present address: Department of Biomolecular Chemistry, Kyoto Prefectural University, Hangi-cho, Shimogamo, Sakyo-ku, Kyoto 606-8522, Japan
[6]Lead Contact
ORCID ID: 0000-0003-0361-3796 (H.M.), 0000-0002-3466-8899 (H.F.).

Running title : High Activity Hybrid-Rubisco

[*]Correspondence: h-matsu@fc.ritsumei.ac.jp (H.M.), fukayama@people.kobe-u.ac.jp (H.F.)

Data deposition: The coordinates and structure factors have been deposited in the Protein Data Bank, www.wwwpdb.org (PDB IDs 6KYI and 6KYJ for WT-Rubisco and CSS-Rubisco, respectively).

Short Summary : Rubisco is a key enzyme of photosynthetic CO_2 fixation. Hybrid Rubisco with replacement of rice Rubisco small subunit with sorghum counterpart expressed in rice exhibited C_4-plant-like high catalytic activity. Transgenic rice expressing the hybrid-Rubisco showed slightly higher photosynthetic capacity. Based on crystal structural analysis, we speculate a possible function of βC-βD hairpin of small subunit in determining the catalytic activity.

ABSTRACT

Photosynthetic rate at the present atmospheric condition is limited by the CO_2-fixing-enzyme ribulose-1,5-bisphosphate carboxylase/oxygenase (Rubisco) because of its extremely low catalytic rate (k_{cat}) and poor affinity for CO_2 (K_c) and specificity for CO_2 ($S_{c/o}$). Rubisco in C_4 plants generally shows higher k_{cat} than that in C_3 plants. Rubisco consists of eight large subunits and eight small subunits (RbcS). Previously, the chimeric incorporation of sorghum C_4-type RbcS significantly increased the k_{cat} of Rubisco in a C_3 plant, rice. In this study, we knocked out rice *RbcS* multigene family by CRISPR/Cas9 and completely replaced the rice RbcS with sorghum RbcS in rice Rubisco. Obtained hybrid-Rubisco showed almost C_4-plant-like catalytic properties, i.e., higher $k_{cat,}$ higher K_c and lower $S_{c/o}$. Transgenic lines expressing the hybrid-Rubisco accumulated reduced levels of Rubisco, whereas these showed slight but significantly higher photosynthetic capacity and similar biomass production under high CO_2 condition compared to wild-type rice. High-resolution crystal structural analysis of the wild-type Rubisco and hybrid-Rubisco revealed the structural differences around the central pore of Rubisco and the βC-βD hairpin in RbcS. We speculate that such differences, particularly in the βC-βD hairpin, may impact the flexibility of Rubisco catalytic site and change the catalytic properties.

INTRODUCTION

The global demand for food and bioenergy from plants is increasing. To meet the demand, the productivity of plants need to be substantially improved, and this requires breakthrough in biotechnology. Because plant biomass and yield depend on photosynthetic activities, many scientists have been challenged to improve photosynthesis using different strategies (Peterhansel and Offermann, 2012; Andralogic et al., 2018). Photosynthesis is a quantitative trait and consists of complex multistep reactions that is controlled by many genes. However, one of the major limiting factors of photosynthesis is the inefficient catalysis of ribulose-1,5-bisphosphate carboxylase/oxygenase (Rubisco) (Sharwood, 2017; Galmés et al., 2019). Rubisco is a key photosynthetic enzyme responsible for CO_2 fixation, but it also catalyses the oxygenation reaction using O_2 as substrate, leading to wasteful photorespiration (Fernie and Bauwe, 2020). Many important crops, such as rice, wheat, and potato, are classified as C_3 plants. The catalytic property of Rubisco in most C_3 plants can be characterized as lower catalytic rate (k_{cat}), lower K_m for CO_2 (K_c) and higher specificity for CO_2 ($S_{c/o}$) compared with that of C_4 plants such as maize and sorghum (Seemann et al., 1984; Sage, 2002; Tcherkez et al., 2006; Ishikawa et al., 2009; Sharwood et al., 2016). To compensate for a slower k_{cat}, C_3 plants accumulate large amount of Rubisco in their leaves, which accounts for 15-30% of the total leaf nitrogen content, leading to a low nitrogen use efficiency (Evans, 1989; Makino et al., 1992). However, higher affinity for CO_2, i.e., lower K_c and higher $S_{c/o}$ can be beneficial for C_3 plants to reduce the photorespiration (Sage, 2002; Ishikawa et al., 2009). Rubisco in C_4 plants showed higher k_{cat}, but the affinity and specificity for CO_2 are lower than that in C_3 plants. The ideal Rubisco would possess catalytic properties which include higher k_{cat}, lower K_c, and higher $S_{c/o}$, whereas a trade-off relationship is observed among these parameters (Tcherkez et al., 2006; Ishikawa et al., 2009). Integrated value, the carboxylation efficiency at 21% O_2 (k_{cat}/K_c^{air}) can be useful for evaluating efficient Rubisco in photosynthesis. According to Sharwood et al., (2016), Rubisco in C_4 monocots including sorghum showed higher carboxylation efficiency than that in C_3 plants and have potential to enhance the photosynthetic rate under ambient CO_2 condition in C_3 plants. Meanwhile, C_4 high activity-type Rubisco originally should be beneficial for the photosynthesis under high CO_2 condition. Increases in the k_{cat} usually decrease the affinity for CO_2 and lead to increases in the photorespiration, whereas the photorespiration will decrease under elevated CO_2 conditions. Thus, C_4 high activity-type Rubisco may also have potential for the improvement of photosynthetic efficiency and plant productivity in the future elevated CO_2 conditions. C_4 plants have a CO_2

concentrating mechanism known as C_4 cycle and elevate CO_2 concentration at the Rubisco site. The acquisition of faster Rubisco contributes to improving the photosynthetic efficiency of C_4 plants (Ghannoum et al., 2005). Naturally, C_4 high activity-type Rubisco can be also useful for the challenge to introduce an operational C_4 photosynthetic cycle into C_3 plants.

In vascular plants, Rubisco consists of eight large subunits (RbcL) and eight small subunits (RbcS) to form an L_8S_8 functional structure. The catalytic site is present in RbcL, hence it contains the amino acids that are important for determining the kinetic properties of Rubisco (Andersson and Backlund, 2008). The introduction of C_4 *Flaveria bidentis* RbcL into tobacco (*Nicotiana tabacum*) significantly increased the k_{cat} of Rubisco (Whitney et al., 2011). Similarly, the k_{cat} of Rubisco could be enhanced by overexpressing either a RbcS from the C_4-plant *Sorghum bicolor* (SbRbcS) (Ishikawa et al., 2011), or a non-photosynthetic cell RbcS isoform (OsRbcS1) in rice (*Oryza sativa*) (Morita et al., 2014). RbcS isoform expressed in trichomes increased the specific activity of Rubisco and also shifted its optimum pH toward acidic in tobacco (Laterre et al., 2017; Lin et al., 2020). Similar effects on Rubisco kinetics was recently reported in potato orthologous RbcS (Martin-Avila et al., 2020). The substitution of native RbcS to foreign RbcS and directed mutagenesis within the RbcS βA-βB loop have also been shown to influence the carboxylation properties, including CO_2-specificity of *Chlamydomonas* Rubisco (Spreitzer, 2003; Genkov et al., 2010). The amino acid sequences of RbcL are highly conserved among plant species, whereas those of RbcS are much more divergent (Andersson and Backlund, 2008). Together, these findings suggest that RbcS can be an important determinant of the kinetic properties of Rubisco, although the amino acids and structural mechanisms influencing the catalytic diversity remain poorly understood.

In this study, we knocked out the rice *RbcS* multigene family in SbRbcS overexpression lines by CRISPR/Cas9 and successfully obtained a complete hybrid Rubisco consisting of rice RbcL and SbRbcS. We studied the biochemical properties and determined the crystal structure of hybrid Rubisco. Based on these results, we hypothesize that L102 in SbRbcS can stimulate the flexibility of Rubisco catalytic site and change its kinetic properties. It was also proposed that our hybrid Rubisco can be useful for the improvement of photosynthesis and biomass production under future elevated CO_2 conditions.

RESULTS

OsRbcS Was Successfully Replaced with SbRbcS in Rice Rubisco

Previously, we showed that the overexpression of SbRbcS using a photosynthetic cell specific prompter (*Cab* promoter) increased the k_{cat} of Rubisco in rice (Ishikawa et al, 2011). In these SbRbcS-overexpression lines (SS lines), Rubisco is present as a chimera of SbRbcS and rice RbcS (Figure 1A). To better understand how SbRbcS imparts this kinetic change requires knockout of endogenous rice *RbcS* genes in SS lines. Rice contains five *RbcS* genes (*OsRbcS1-5*). Among them, *OsRbcS*1 is not expressed in photosynthetic cells (Morita et al., 2014). Thus, in this study, *OsRbcS2-5* multigene knockout was carried out utilizing off-target mutations by CRISPR/Cas9 system (Supplemental Figure 1A). Analysis of nucleotide sequence of two transgenic lines (CSS16 and CSS10) revealed that all of *OsRbcS2-5* contained biallelic frameshift mutations at the region of CRISPR/Cas9 target sequence (Supplemental Figure 1B). SDS-PAGE analysis showed that both OsRbcS and SbRbcS were detected in SS lines, whereas OsRbcS was undetectable and completely replaced with SbRbcS in CSS lines (Figure 1B). Thus, two CSS lines achieving *OsRbcS2-5* multigene knockout were successfully obtained. We confirmed that there were no mutations in four potential off-target sites of rice genome detected by CRISPR-P (Lei et al., 2014) (Supplemental Figure 2). These plants basically did not exhibit an abnormality in growth behavior or morphology (Figure 1C). Through genetic segregation, CSS lines carrying the mutations in *OsRbcS*s without the CRISPR/Cas9 transgene were obtained and its T_3 generations were used for subsequent experiments.

Rubisco Content Decreased in CSS Lines

Rubisco content was significantly decreased in CSS lines (Figure 2). CSS16 and CSS10 expressed 44% and 67% of Rubisco in WT, respectively. Thus, CSS10 accumulated more Rubisco than CSS16. These Rubisco contents were largely consistent with SbRbcS levels of their parent lines i.e., SS16 and SS10 (Figure 1B; Ishikawa et al., 2011). In addition, the Rubisco contents among genotypes were well correlated with the transcript levels of total *RbcS* (*OsRbcS* or *SbRbcS*), suggesting that Rubisco contents in CSS lines were largely determined by the available amount of SbRbcS that corresponded to the abundance of transcript (Supplemental Figure 3). The contents of nitrogen and soluble protein were decreased in CSS16 and CSS10 (Figure 2), possibly due to a large decrease in the Rubisco contents. In contrast, the chlorophyll content in CSS lines was at similar level to that in WT.

Replacement of OsRbcS with SbRbcS Significantly Increases k_{cat} and K_c

Rubisco activities were determined at different CO_2 concentrations and using these data, the k_{cat} and K_c were calculated (Figure 3A-3B). The k_{cat} of Rubisco was significantly increased in CSS lines compared with WT. The k_{cat} in CSS lines was 1.8-1.9 times that in WT which accounted for 78% of sorghum Rubisco. This increase in k_{cat} is greater than that in simple SbRbcS overexpression lines, i.e., SS lines which showed at most 1.5 times higher k_{cat} than WT (Ishikawa et al, 2011). The K_c and K_c at 21% O_2 (K_c^{air}) of Rubisco in CSS lines also increased 1.9 and 2.1 times those in WT, respectively. Concomitant with this increase in K_c, the specificity factors ($S_{c/o}$) in CSS lines were reduced to 83-86% of WT. These are typical characteristics of C_4 plant Rubisco (Hermida-Carrera et al. 2016). However, the CSS lines maintained similar levels of carboxylation efficiency (k_{cat}/K_c) as WT, which were significantly higher than that in sorghum. The k_{cat}/K_c^{air} in CSS lines showed intermediate values between WT and sorghum. In contrast to these differences in k_{cat} and K_c, the K_m for ribulose-1,5-bisphosphate (RuBP) was at similar levels in all genotypes. Although the k_{cat} of CSS lines was still lower than that in sorghum, these findings clearly demonstrate that the incorporation of SbRbcS shifts the kinetic properties to increase the activity of Rubisco, and RbcS is a key determinant of Rubisco kinetic properties.

CSS lines showed similar rate constants for photosynthetic activation after step increase in light intensity with WT (Supplemental Figure 4). Moreover, Rubisco activation states in CSS lines were higher than that in WT both under ambient and high CO_2 conditions. These results strongly suggest that Rubisco activase in rice can properly activate hybrid-Rubisco expressed in CSS lines. It was reported that Rubisco activation state increased in RbcS antisense tobacco with reduced Rubisco content (Quick et al. 1991). Therefore, higher Rubisco activation states observed in CSS lines can be due to reduced Rubisco content and/or increased Rubisco activase : Rubisco ratio.

CSS10 Showed Higher Photosynthetic CO_2 Assimilation Rate than WT under High CO_2 Condition

Because CSS lines have less Rubisco contents, the photosynthetic CO_2 assimilation rates under less than ambient CO_2 partial pressures (40 Pa) were lower than those in WT (Figure 4). This decrease was significant in CSS16, a line expressing lower amount of Rubisco. The carboxylation efficiency is an important determinant of CO_2 assimilation rate under low CO_2 condition (Galmes et al. 2014; Sharwood et al. 2016). Thus, increase in K_c and concomitant

decrease in the carboxylation efficiency (Figure 3) reduces the photosynthetic rate under ambient CO_2 condition in CSS lines. In contrast, the photosynthetic rates at high CO_2 condition (100 Pa) in CSS lines were similar to those in WT (Figure 4). Although there was no significant difference, CSS10 exhibited slightly higher V_{cmax} and J_{max} than WT (Supplemental Figure 5), suggesting that the potentials of RuBP carboxylation and RuBP regeneration would increase in CSS10. In addition, because of its low nitrogen content, CSS10 showed slight but significantly higher photosynthetic rate based on the nitrogen content at high CO_2 condition than WT. Increase in the photosynthetic rates at high CO_2 condition of CSS10 based on nitrogen were 12.3%. Although higher Rubisco activation state observed in CSS lines compared to WT can also contribute to this high photosynthetic rate under high CO_2 condition (Supplemental Figure 4), these results suggest the usefulness of our transgenic plants, introducing high activity type Rubisco to improve the photosynthetic nitrogen use efficiency of C_3 plants under elevated CO_2 condition.

Decrease in Dry Matter Productions in CSS Lines Were Restored to WT Level by Elevated CO_2 Treatment

CSS lines were grown in a growth chamber under ambient (40 Pa) and elevated (100 and 300 Pa) CO_2 conditions for a relatively short period and the plant length, leaf number, and tiller number were determined (Supplemental Figure 6). The plant length and leaf number in CSS lines were at similar levels to those in WT, both under ambient and elevated CO_2 conditions. Under ambient CO_2 condition, the tiller number in CSS16 was significantly lower than that in WT. However, the tiller numbers in CSS16 were recovered to the level of WT under elevated CO_2 conditions. Moreover, CSS10 showed significantly higher tiller numbers at the final time points than WT under the conditions. This trend was more clear under CO_2 partial pressure of 300 Pa. The dry weights of leaf blade, leaf sheath and root in CSS lines under ambient CO_2 were significantly lower than that in WT (Figure 5). The total dry weights of CSS16 and CSS10 were reduced to 50 and 70% of WT, respectively. The decrease in dry weights were well correlated with Rubisco contents and photosynthetic rate under ambient CO_2 condition (Figures 2 and 4). Thus, it was considered that these reduced growth performance in CSS lines were largely due to lower photosynthetic rates under ambient CO_2 condition (Figure 4). Although the root dry weight was still lower in CSS lines, the dry weights of other organs and total dry weight in CSS lines were almost recovered to the level of WT under elevated CO_2 conditions. Rubsco contents in CSS16 and CSS10 grown under elevated CO_2 (100 Pa) were 36

and 56% of WT, respectively and slightly lower than those under ambient CO_2 condition (Figure 2 and Supplemental Figure 7). However, similar to ambient CO_2 grown plants, the photosynthetic rates at high CO_2 condition based on nitrogen content in CSS line grown under elevated CO_2 condition were higher than that in WT (Figure 4 and Supplemental Figure 8). The contents of leaf constituents (Rubisco, chlorophyll, soluble protein and nitrogen) and photosynthetic rate of plants grown under CO_2 partial pressure of 300 Pa were not determined because some abnormality in leaf development was observed at the later growth stage under the condition. Rubisco activation at high CO_2 condition (100 Pa) was higher in CSS lines than that in WT (Supplemental Figure 4). This high Rubisco activation can be beneficial to support photosynthesis. In contrast, Rubisco seems to be excess in WT under high CO_2 condition. Thus, CSS lines contains substantially reduced levels of Rubisco while also maintaining normal level of biomass production by sufficient photosynthetic activity under elevated CO_2 conditions.

Number of Sulfate Ion Bound to Catalytic Site of Rubisco and the Structure around the Solvent Channel Were Different between WT-Rubisco and CSS-Rubisco

WT-Rubisco and CSS-Rubisco were purified from rice leaves in the same procedure described in the previous studies for rice Rubisco (Matsumura et al., 2012). Both Rubiscos were crystallized using the same reservoir condition (see Materials and Methods), and their structures were determined at resolutions of 1.75 and 1.70 Å, respectively (Supplemental Table 1).

WT-Rubisco crystals belonged to space group *I*4, with two large subunits (RbcL; chains A and B) and two small subunits (RbcS; chains S and T) in the asymmetric unit (Supplemental Figures 9A-9B). As the crystallization solution contained sulfate ions, the structure included sulfate ions at the binding sites of phosphate group of RuBP. This active site of chain A contained two sulfate ions which were located in P1 distal subsite and P2 upper subsite (Figure 6A and Supplemental Figure 10A). Generally, Rubisco undergoes a disorder-order transition of four RbcL regions of residues around 1-20 (N-terminal segment), 64-67 (60s loop), 332-337 (loop 6), and 464-475 (C-terminal tail) from the open to closed state of the active site, which correlates with the absence or presence of the sugar phosphate substrate (or the transition state analogue 2-carboxy-D-arabinitol-1,5-bisphosphate (2CABP)) (Duff et al., 2000). The active site of chain A has structurally ordered 60s loop (in chain B) but disordered N-terminal segment, loop 6, and C-terminal tail. The active site of chain B contained only one sulfate, which bound to P2 upper subsite (Figure 6A), and all four regions (N-terminal segment, 60s

loop (in chain A), loop 6, and C-terminal tail) were disordered (Supplemental Figure 10B). The remarkable differences in those two structures were not observed because the root mean square deviations (rmsd) of 428 Cα atoms of RbcL and 119 Cα atoms of RbcS between two forms were relatively small, 0.319 and 0.195 Å, respectively. Only the slight structural difference in two RbcLs was observed on a loop of residues, 90-97, that is responsible for the interaction with Rubisco activase (Portis et al., 2008). This structural difference is likely caused by crystal packing, as shown in Supplemental Figure 11; however, the other structural features describing in this manuscript are unlikely influenced by crystal packing, as we carefully inspected. Although the carbamylation of K201 is necessary for Rubisco activation, K201 in chains A and B were not carbamylated, because Mg^{2+} and HCO_3^- were not included in the reservoir solution of crystallization.

The crystal structure of CSS-Rubisco, first for the vascular plant hybrid-Rubisco, basically resembled that of WT-Rubisco. CSS-Rubisco crystals belonged to space group $P42_12$, with four RbcL chains (A, C, E, and G) and four RbcS chains (S, U, W, and Y) in the asymmetric unit (Supplemental Figures 9C-9D). The four RbcLs could be superimposed well (rmsd of 0.137-0.196 Å for 446-448 Cα atoms), whereas the structural difference between four RbcSs was relatively larger (rmsd of 0.159-0.324 Å for 119-120 Cα atoms). The large structural difference between the four RbcS was found in the N- terminal residues 1-23, C-terminal tails of residues 118-121, and a region of residues 91-95, that contacted a symmetry-related adjacent molecule, and a region of residues 48-49, that had alternative conformations (Figure 6B); in other words, the electron density map allowed the residues 48-49 to be placed in two different orientations, each with 50% occupancy. The observed conformation was basically the same in the four copies of CSS-Rubisco in the crystal asymmetric unit, indicating that it does not result from crystal-packing interactions. Electron density maps indicated that RbcS of CSS-Rubisco was completely replaced with the amino acids corresponding to those of SbRbcS (Supplemental Figure 13). The active sites of all CSS-Rubisco RbcL contained two sulfate ions (Figure 6A), i.e., in P1 distal subsite and P2 upper subsite similar to chain A of WT-Rubisco. CSS-Rubisco had disordered N-terminal segment and C-terminal tail, but ordered loop 6 and 60s loop (in neighboring subunit). Similar to WT-Rubisco, K201 was not carbamylated in CSS-Rubisco.

Structural comparison between CSS-Rubisco and WT-Rubisco shows that the RbcL of CSS-Rubisco is similar to both chains A and B of WT-Rubisco RbcL (rmsd of 0.234-0.268 and 0.294-0.340 Å for 428 Cα atoms, respectively). On the other hand, rmsd of RbcS between WT-Rubisco and CSS-Rubisco were relatively large (0.330-0.424 Å for 119 Cα atoms),

because 28 of the 122 amino acids of RbcS were different. Notable differences in RbcS between WT-Rubisco and CSS-Rubisco were found in residues 7-9 (rmsd of 0.92 Å for 3 Cα atoms) and 48-49 (rmsd of 0.73Å for 2 Cα atoms) (Supplemental Figure 14A). The residues 7-9 was located at the edge of the solvent channel (central pore of Rubisco), and the residues 48-49 had alternative conformations in RbcS of CSS-Rubisco not of WT-Rubisco (Figure 6B). The region of residues 48-49 also formed a solvent channel and was located in the βA-βB loop.

Comparing the structures of sulfate ion-bound WT-Rubisco in this study and 2CABP-bound WT-Rubisco reported previously (Matsumura et al., 2012), we formulate a hypothesis. During catalysis, the conformational changes in Rubisco can occur not only in N-terminal segment, 60s loop, loop 6, and C-terminal tail, but also in the main chain of the region of residues 102-114 in β hairpin (βC-βD) of the adjacent RbcS (Figure 7A-7C). The substrate binding causes the closure of the catalytic loops, thereby leading to slight changes in the direction of the side chain of L74 on the 60s loop of RbcL (Figure 7C). As a result, F104 of the adjacent RbcS which was sandwiched by L74 and I102 would incline, leading to a large structural change in the main chain of the βC-βD (Figure 7C and Supplemental Figure 14B). Interestingly, in WT-Rubisco, F104 was sandwiched by I102 and L74 whereas the residue of I102 was substituted by leucine in CSS-Rubisco containing SbRbcS (Figure 7D-7F). In WT-Rubisco, the C-C distances of I102-F104 (the distance between Cδ1 in I102 and Cε2 or Cζ in F104) were 3.58-3.72 Å, while the C-C distances (distance between Cδ1 or Cβ in L102 and Cε2 or Cζ in F104) of L102-F104 were 4.11-4.28 Å in CSS-Rubisco (Supplemental Figure 15). We hypothesize that this difference in distance between amino acids would affect the flexibility of the 60s loop and then the catalytic turnover of Rubisco.

Amino acid sequence of RbcS was analyzed in 162 plant species (Supplemental Table 2). Most of C_3 plants (97%) contain I102. Among 128 C_3 plants, L102 is only found in four C_3 species, *Dichanthelium oligosanthes*, *Ipomoea batatas*, *Ipomoea triloba* and *Thyridolepis mitchelliana*. Interestingly, *Ipomoea batatas* showed higher k_{cat} among C_3 plants (Hermida-Carrera et al., 2016). In contrast to C_3 plants, 44% of C_4 plants (among 34 species) contain L102. In general, many C_4 monocots have efficient high k_{cat} Rubisco (Sharwood, 2017). If limited to C_4 monocots, the proportion of L102 increases to 67%. Therefore, L102 is considered to be abundant in C_4 monocots.

DISCUSSION

In our previous work, the chimeric incorporation of SbRbcS was shown to enhance the k_{cat} of

Rubisco in rice (Ishikawa et al, 2011). In this study, we successfully knocked out rice RbcS to produce complete hybrid Rubisco consisting of rice RbcL with SbRbcS (Figure 1B). This hybrid Rubisco brought more clear results, i.e., it showed approximately two times higher k_{cat} than WT (Figure 3), it corresponded to the same level in C_4 plants (Sharwood, 2017). To our best knowledge, there have been no reports of increasing k_{cat} to this level successfully by genetic recombination. Concomitant with this increase in k_{cat}, K_c was increased and $S_{c/o}$ was decreased like a C_4 plant Rubisco (Figure 3). The importance of RbcS in determining the catalytic properties of Rubisco has also been suggested by hybrid Rubisco of *Chlamydomonas* RbcL with RbcS from different species (Genkov et al., 2010). Putting all of these into perspective, RbcS must be an important determinant of Rubisco kinetic properties.

The role of RbcS in Rubisco catalysis has been studied using the RbcS defective mutant of *Chlamydomonas* expressing foreign or mutant RbcS (Spreitzer, 2003; Genkov et al., 2010). It was shown that the substitution of the amino acid residues in the βA-βB loop of RbcS, where the regions around solvent channels significantly affect the kinetic properties of Rubisco (Genkov et al., 2010; Karkehabadi et al., 2005; Esquivel et al., 2013). For example, R53 and R65 in βA-βB loop were considered to be important in the interaction with RbcL and could influence the catalytic properties (Spreitzer et al., 2001; Spreitzer, 2003). However, these amino acids are conserved in OsRbcS and SbRbcS (Supplemental Figure 12). In the RbcS of WT-Rubisco and CSS-Rubisco, the regions of residues 7-9 and 48-49 (in βA-βB loop) located around the solvent channel showed relatively large structural differences (Figure 6B and Supplemental Figure 14A). Particularly, E48 in βA-βB loop of SbRbcS is different from OsRbcS2-5 and common to OsRbcS1 which also enhances the k_{cat} of rice Rubisco (Morita et al., 2014). E48 is placed on the surface of the solvent channel (Figure 6B). However, it was reported that the structure of surface at the opening of central solvent channel can affect the kinetic properties (Esquivel et al., 2013). Thus, the differences in the amino acid residues around central solvent channels in SbRbcS may enhance the k_{cat} in CSS-Rubisco.

In this study, we speculate another possibility. The coordinated structural changes in βC-βD of adjacent RbcS of rice Rubisco are shown in this study (Figure 7A-7B). In the structural change in βC-βD, the side chain of F104, which was sandwiched between I102 and L74 by hydrophobic interactions, should structurally incline (Figure 7C). This structural change requires disruption of the hydrophobic interactions between the side chain of F104 and the side chain of I102 in WT-Rubisco. In RbcS of CSS-Rubisco, the substitution of I102 with leucine occurs, and interactions between L102 and F104 are considered to be weaker than those of WT-Rubisco, judging from the C-C distances (Supplemental Figure 15). Therefore, the

interactions between L102 and F104 in CSS-Rubisco are easily disrupted. Thus, F104 side chain may undergo structural change more smoothly in CSS-Rubisco than that in WT-Rubisco; as a consequence, the k_{cat} can be increased in CSS-Rubisco. Considering together, the substitution of I102 with leucine may increase the flexibility of catalytic loops, particularly 60s loop.

Generally, C_4 plants with high k_{cat} Rubisco at low content show higher photosynthetic rate and growth performance under ambient CO_2 condition, because they acquired CO_2 concentrating mechanism to enhance the photosynthesis (Sharwood, 2017). CSS lines also have C_4-plant like Rubisco (Figure 3), whereas they showed lower photosynthetic rate and biomass production than WT under ambient CO_2 condition (Figure 4 and 5), because of having no CO_2 concentrating mechanism. Previously, we found that the enhancement of k_{cat} by introducing a SbRbcS or OsRbcS1 alone did not improve the photosynthetic performance of rice at various CO_2 conditions (Ishikawa et al., 2011; Morita et al., 2014). In these studies, foreign *RbcS* was overexpressed in rice leaves while the native rice *RbcS* remained functional. Thus, Rubisco contents were significantly increased and become excess in these plants. Consistent with this observation, Rubisco activation was reduced in SbRbcS overexpression lines (Ishikawa et al., 2011). Decrease in carboxylation efficiency observed in CSS-Rubisco (Figure 3) could have a negative effect on the photosynthetic rate around ambient CO_2 condition. For these reasons, it is considered that the photosynthetic rate did not increase in those transgenic plants. Considering the kinetic properties, our hybrid-Rubisco is beneficial for high CO_2 condition. However, the photosynthetic rate is essentially not limited by the Rubisco activity under high CO_2 conditions. In order to increase the photosynthetic rate at elevated CO_2 levels, the RuBP regeneration capacity should be enhanced. Interestingly, one of the transgenic lines, CSS10, showed somewhat higher photosynthetic rate at high CO_2 condition (Figure 4), even though the expression level of Rubisco of this line is 67% of WT (Figure 2). These phenotypes are largely consistent with those of a simple antisense transgenic rice, which exhibits 65% Rubisco level of WT (Makino et al., 1997). In this antisense plants, some photosynthetic components such as chlorophyll, cytochrome f and coupling factor 1 were increased, suggesting an increase in the allocation of nitrogen due to a reduction in the Rubisco to other photosynthetic components. Therefore, it is expected that an increase in the allocation of nitrogen to some photosynthetic components determining the RuBP regeneration capacity would occur in CSS lines. However, the CSS lines examined herein did not exhibit increases in chlorophyll content (Figure 2). The nitrogen content was decreased in CSS lines (Figure 2), and this decrease was not observed in RbcS antisense rice (Makino et al., 1997). A reduction in

Rubisco could exert negative secondary effects on leaf constituents (Matt et al., 2002). Thus, fine tuning the balance between the Rubisco capacity and its effects on photosynthesis seems important to enhance the photosynthetic capacity. In addition, to further enhance the photosynthetic capacity of CSS lines, it is necessary to find out the way to preferentially increase the allocation of nitrogen to RuBP regeneration related proteins.

Although CSS10 showed slightly higher photosynthetic rate under high CO_2 condition than WT, the dry weight was not increased in CSS lines compared with WT (Figure 4 and 5). The photosynthetic rate in Figure 4 was determined under the condition of nearly light saturation (photosynthetically active photon flux density (PPFD) of 1,500 μmol m^{-2} s^{-1}; see Supplemental Figure 16) using uppermost fully expanded leaves. However, we grew rice plants with subsaturating light intensity (PPFD of 800 μmol m^{-2} s^{-1}) and the light intensity should be weaker at the lower positioned leaves. Under light limited condition, C_3-type Rubisco with higher affinity for CO_2 rather than C_4-type Rubisco with high k_{cat} suggested to be advantageous for photosynthesis (Long et al., 2006). However, under high CO_2 condition, CSS lines showed similar photosynthetic rate under limited light intensity (Supplemental Figure 16), suggesting that CSS-Rubisco should be sufficiently efficient under high CO_2 and light limited conditions. Growth phenotype of antisense RbcS rice lines under elevated CO_2 was largely similar to CSS lines (Makino et al., 2000; Figure 5). Thus, both the content of Rubisco and the catalytic properties contribute to the growth phenotype of CSS lines, whereas the former might be a larger determinant.

Recently, considerable progress has been made in the understanding of Rubisco biosynthesis and its engineering (Aigner et al., 2017; Bracher et al. 2017). Cyanobacterial high activity-type Rubisco was functionally expressed in tobacco by the coexpression of assembly chaperone RbcX or carboxysomal protein CcM35 (Lin et al., 2014). The expression of hybrid Rubisco, consisting of *Arabidopsis* RbcL and tobacco RbcS, was effectively enhanced by the co-expression of another chaperon, RAF1, from *Arabidopsis* (Whitney et al., 2015). RAF1 also increased the Rubisco content in maize RbcL and RbcS overexpression lines (Salesse-Smith et al., 2018). Moreover, the expression of functional plant Rubisco in *Escherichia coli* was succeeded by the coexpression of five chloroplast chaperones (Aigner et al., 2017). This will allow for the systematic selection of efficient Rubisco for the improvement of photosynthesis. Thus, the introduction of genetically distant and efficient Rubisco into vascular plants is now close to becoming reality. However, considering the interaction with assembly chaperones and Rubisco activase in host plants, the introduction of Rubisco from a genetically similar species is preferable. In this situation, C_4 plants must serve as useful genetic resources that are

distributed across a wide range of species, consisting of approximately 7500 species (Sage et al., 2011). Therefore, C_4 plants are available to provide suitable high activity-type RbcS depending on host plants. The introduction of a C_4-RbcS into C_3 plants can be a promising strategy to improve the kinetic properties of Rubisco and may lead to the improvement of photosynthesis and productivity in the future.

METHODS

Plant materials and growth conditions

Rice (*Oryza sativa* L. cv. Nipponbare) and its transgenic lines were grown in a growth chamber on a 30˚C/25˚C night cycle with a day period of 14 h under illumination at PPFD of approximately 800 μmol m^{-2} s^{-1} at the uppermost leaf. Rice seedlings at the leaf stage (number of leaves in the main stem) of 4.5 were transplanted into 1 L pots filled with paddy soil containing a chemical fertilizer (N:P:K=8:8:8) at 0.3 g N, a micronutrient at 0.15 g and a silicate fertilizer at 1.5 g per pot. At the panicle initiation stage, the same chemical fertilizer was applied at a rate of 0.1 g N as a top dressing. To determine the Rubisco, soluble protein, chlorophyll and nitrogen, the leaves were harvested after measuring the gas exchange rate. For the determination of Rubisco kinetics, sorghum (*Sorghum bicolor* L. cv. Tentaka) and rice were planted into 1 L pots filled with a commercial culture soil and paddy soil as above, respectively, and grown in a temperature-controlled greenhouse on a 30°C day/25°C night cycle. The leaves were sampled at 10:30–11:30 on sunny days. After sampling, the leaves were immediately frozen in liquid nitrogen and stored at -80°C until required.

The CO_2 treatment (38 and 100 Pa as ambient and elevated CO_2, respectively) was started immediately after germination. Thirty days after germination, shoot and root were sampled and dried for three days at 80˚C to determine the dry weight.

Knockout of *OsRbcSs* by CRISPR/Cas9

The plasmid construction for multigene knockout of *OsRbcSs* was carried out basically as described previously (Mikami et al., 2015). Target sequence created from two primers (Supplemental Table 3) was cloned into the vector pZK_OsU6-gRNA. Connected DNA fragment of *OsU6* promoter, target sequence, sgRNA scaffold and poly(T) was obtained from the digestion of the vector by *I-SceI* and inserted into *I-SceI* site of binary vector

pZH_MMCas9 containing acetolactate synthase (ALS) expression cassette. The construct was introduced into calli derived from the transgenic line SS16 and SS10, which overexpresses SbRbcS[15] via *Agrobacterium*-mediated gene transfer. Bialaphos-resistant transgenic plants were regenerated from calli and planted in soil as above.

SDS-PAGE analysis

The leaves were homogenized in extraction buffer containing 50 mM Hepes-KOH, 10 mM $MgCl_2$, 1 mM EDTA, 5 mM DTT, 0.01 mM leupeptin, 1 mM phenylmethylsulfonylfluoride, 10% (w/v) glycerol and 5% (w/v) polyvinylpolypyrrolidone, pH 7.4, using a cold mortar and pestle with a small amount of quartz sand. The homogenate was centrifuged at 15,000 × g for 5 min at 4°C, and the supernatant was collected, which represented the total soluble protein extract. SDS-PAGE was performed using a 14% (w/v) gel. After SDS-PAGE, the gel was stained with Coomassie Brilliant Blue R-250.

Measurement of Rubisco Activity

The leaves were homogenized in extraction buffer containing 100 mM Bicine-NaOH, 1 mM EDTA, 5 mM $MgCl_2$, 2 mM NaH_2PO_4, 0.4% (w/v) bovine serum albumin, 5 mM DTT, 4 mM amino-n-caproic acid and 0.8 mM benzamidine, pH 8.0, using a chilled mortar and pestle. For analysis of K_m for RuBP, NaH_2PO_4 was omitted from the extraction buffer. The homogenate was then centrifuged at 15,000 × g for 2 min at 4°C. The Rubisco in the supernatant was activated by pre-incubation with 15 mM $MgCl_2$ and 5 mM $NaHCO_3$ on ice for 15 min. The Rubisco activity was determined at 28°C using [^{14}C] $NaHCO_3$ (specific activity, 37 MBq $mmol^{-1}$) by assaying the incorporation of ^{14}C into acid-stable products, as described previously (Ishikawa et al., 2009). The reaction was started by the addition of activated Rubisco to a reaction mixture containing 100 mM Bicine-NaOH, 20 mM $MgCl_2$, 1 mM EDTA-Na, 5 mM DTT, 12.5-400 μM RuBP, 0.5-15 mM $NaH^{14}CO_3$ and 1.0 W-A units carbonic anhydrase, pH 8.2. After 1 min, 1/2 volume of 1 N HCl was added to the reaction solution to stop the reaction. The acidified reaction mixes were dried and acid-stable ^{14}C was measured by liquid scintillation.

The Rubisco catalytic site concentrations were determined by measuring the stoichiometric binding of [^{14}C] 2CABP (specific activity, 1.85 GBq $mmol^{-1}$) as described previously (Ishikawa et al., 2009).

The k_{cat} and K_c were calculated from the Hanes-Woolf plot of the Rubisco activities at six different $NaH^{14}CO_3$ concentrations (0.5-15 mM). The CO_2 concentrations in the assay mixture were calculated using pKa for bicarbonate of 6.100-6.108 depending on ionic strengths. For determination of K_c and K_c^{air}, the reaction mixtures were equilibrated with N_2 and 21% O_2 with N_2, respectively. The K_m for RuBP was calculated from the Hanes-Woolf plot of the Rubisco activities at six different RuBP concentrations (12.5-400 μM).

Measurement of photosynthetic rate

The gas-exchange of the uppermost fully expanded leaf was measured using an open gas-exchange system (LI-6400, Li-Cor, Lincoln). The measurement was performed at a leaf temperature of 28°C, 21% O_2, a PPFD of 1500 μmol quanta m^{-2} s^{-1}, a leaf-to-air vapor pressure difference of 1.0-1.2 kPa and CO_2 partial pressures of 4.5-100 Pa. To determine Rubisco CO_2/O_2 specificity ($S_{c/o}$), CO_2 compensation points were measured by the gas exchange rates under the condition as described above with four different O_2 partial pressures ranging from two to 20%. The $S_{c/o}$ was estimated by the slope of the regression lines of the dependence of CO_2 compensation point on the O_2 concentration (Laisk and Loreto, 1996).

Determination of the contents of Rubisco, soluble protein, chlorophyll and nitrogen

The contents of Rubisco, soluble protein and chlorophyll in the leaves were determined basically as described previously (Ishikawa et al., 2011). The leaf tissues were homogenized in extraction buffer containing 50 mM Hepes-KOH, 5 mM $MgCl_2$, 1 mM EDTA, 5 mM DTT, 4 mM amino-n-caproic acid, 0.8 mM benzamidine, 0.05% (v/v) Triton X-100, 5% (w/v) glycerol and 0.1% (w/v) polyvinylpolypyrrolidone, pH 7.4, using a chilled mortar and pestle with a small amount of quartz sand. The homogenate was then centrifuged at 15,000 × g for 5 min at 4°C. The supernatant was used to determine the contents of Rubisco and total soluble proteins. The Rubisco content was determined using [^{14}C] 2CABP as described above. The total soluble protein was determined by colorimetric assay with bovine serum albumin as the standard (Bradford, 1976). To determine the chlorophyll content, a portion of the homogenate was removed from the mortar and extracted with 80% (v/v) acetone. The chlorophyll was then determined spectrophotometrically (Porra et al., 1989). The nitrogen content was determined by colorimetric assay after the Kjeldahl digestion of leaf tissues (Willis et al., 1989).

Purification and crystallization

WT-Rubisco and CSS-Rubisco were purified from wild-type and transgenic rice leaves in the same procedure described in the previous studies for rice Rubisco (Matsumura et al., 2012). The crystals were grown at 293 K by hanging-drop vapor diffusion. To crystallize, we prepared purified WT-Rubisco and CSS-Rubisco in solution containing 80 mM Hepes-KOH (pH 8.0), 1 mM EDTA, and 5 mM DTT to 17.5 and 16.5 mg mL^{-1}, respectively. Both crystals were obtained in a week using the same reservoir of the condition of 0.1 M Tris-HCl (pH 9.0), 0.2 M lithium sulfate, 15 % (w/v) polyethylene glycol 4000, and 10 % (w/v) glycerol.

Data collection, structure determination, and refinement

Both crystals were flash-frozen after briefly soaking in a cryoprotectant solution containing 0.1 M Tris-HCl (pH 9.0), 0.2 M lithium sulfate, 15 % (w/v) polyethylene glycol 4000, and 30 % (w/v) glycerol. X-ray diffraction intensities were measured at SPring-8 BL26B1 (Hyogo, Japan) under cryogenic nitrogen gas stream at 100 K. Diffraction data were processed and scaled with XDS (Kabsch, 2010). The phases for both the enzymes were determined by molecular replacement with Molrep in the CCP4 suite (Anonymous, 1994) using the previously determined structure of rice Rubisco–6-phosphogluconate complex (PDB entry: 3AXM) (Matsumura et al., 2012) as a search model. The both models were refined with Refmac5 (Murshudov et al., 2011) and PHENIX (Adams et al., 2010), with manual modification using COOT (Emsley and Cawtan, 2004). The refined structures were validated with MolProbity (Chen et al., 2010). Secondary structural elements were determined with the DSSP algorithm (Kabsch and Sander, 1983). Data collection and refinement statistics are summarized in Supplemental Table 1. The final atomic coordinates and structure factor amplitudes have been deposited in the RCSB Protein Data Bank (PDB entries: 6KYI and 6KYJ). Figures were prepared with PyMOL (Schrödinger).

Data Availability Statement: The atomic coordinates and experimental data submitted to Protein Data Bank will be released to the public immediately after the publication of the paper.

SUPPLEMENTAL INFORMATION

Supplemental Information is available at Molecular Plant Online.

FUNDING

This work was supported by Grants-in-Aid for Scientific Research (17H05732, 18K06094, 19H04735, 19K07582 to H.M.; 24580021, 15H04443 to H.F.); the Program for the Third-Phase R-GIRO Research from the Ritsumeikan Global Innovation Research Organization, Ritsumeikan University; the Cooperative Research Program of Institute for Protein Research, Osaka University (CR-18-05 and CR-19-05); Platform Project for Supporting Drug Discovery and Life Science Research (Basis for Supporting Innovative Drug Discovery and Life Science Research (BINDS)) from AMED under Grant Number JP19am0101070 (to H.M.). This work has been performed under the approval of the Photon Factory and SPring-8 Program Advisory Committee (Proposal Nos. 2017A6748, 2017A2570, 2017B6748, 2018A2719, 2018A6859 and 2017G702).

AUTHOR CONTRIBUTIONS

H.M. and H.F. designed research; H.M., K.S., A.Y., N.K., T.Y., S-i.T., H.Y., M.E., H.F. performed research; H.M., T.Y., S-i.T., H.F. analyzed data; and H.M. and H.F. wrote the paper. The authors declare no conflict of interest.

ACKNOWLEDGEMENT

We thank Prof. Makoto Matsuoka (Nagoya University, Japan) for generous gifts of vectors. We thank Prof. Tetsushi Azuma, Dr. Tomoko Hatanaka and Dr. Daisuke Sasayama (Kobe University) for discussion.

FIGURE LEGENDS

Figure 1. OsRbcS Was Successfully Replaced with SbRbcS in Rice Rubisco.
(A) A schematic representation of our experimental strategy. Transgenic rice plants overexpressing the SbRbcS (SS) were produced. In these plants, both SbRbcS and OsRbcS were expressed. Then, OsRbcS was knocked out by CRISPR/Cas9 to produce transgenic lines achieving complete replacement of OsRbcS with SbRbcS (CSS).
(B) Expression of RbcS in SS and CSS lines analyzed by SDS-PAGE. Soluble proteins (6.4 μg) extracted from uppermost fully expanded leaves were separated by 14 % SDS-PAGE and stained by Coomassie Blue. Fractions around RbcL (upper panel) and RbcS (lower panel) are shown.
(C) Photograph of CSS lines grown for 40 days after seeding. Scale bar = 10 cm.
CSS10 and CSS16, transgenic rice plants expressing the SbRbcS with OsRbcS knockout; OsRbcL, rice RbcL; Sb, sorghum; WT, non-transgenic rice.

Figure 2. Rubisco Content Decreased Significantly in CSS Lines Plants were grown under ambient CO_2 (40 Pa) condition. Uppermost fully expanded leaves at 10.5 leaf stage were used for experiments. Contents of Rubisco, chlorophyll, total soluble protein, and nitrogen in CSS lines are shown. Rubisco contents were 3.76, 1.65 and 2.51 g m^{-2} (55.6, 24.4 and 37.1 μmol catalytic site m^{-2}) for WT, CSS16 and CSS10, respectively. Data represent means ±SD of five biological replicates. Different letters above the bars indicate significant difference ($P < 0.05$) between lines determined by Tukey's test.

Figure 3. Replacement of OsRbcS with SbRbcS Significantly Increases k_{cat} and K_c
(A) k_{cat} and K_c of Rubisco. The catalytic rates of Rubisco in WT, CSS lines and sorghum were determined at different CO_2 concentrations. Using these data, the k_{cat}, K_c and k_{cat}/K_c were calculated.
(B) Summary of Rubisco kinetic properties. K_c^{air} is K_c at 21% O_2. Data represent means ± SD of four to six biological replicates. Different letters indicate significant difference ($P < 0.05$) determined by Tukey's test. nd, not determined.

Figure 4. CSS10 Showed Higher Photosynthetic CO_2 Assimilation Rate than WT under High CO_2 Condition

(A) The dependence on Ci of photosynthetic CO_2 assimilation rates.
(B) The CO_2 assimilation rates at ambient CO_2 (40 Pa) and high CO_2 (100 Pa) conditions. The data are obtained from Figure 4A.
Rice plants were grown in a growth chamber under ambient CO_2 (40 Pa) condition. The uppermost fully expended leaves at 10.5 leaf stage were used for the measurement of photosynthetic rate. The photosynthetic rates based on the leaf area (upper panel) and nitrogen (lower panel) are shown. Data represent means ± SD of four to five biological replicates. Different letters indicate significant difference ($P < 0.05$) determined by Tukey's test.

Figure 5. Decrease in Dry Matter Productions in CSS Lines Were Restored to WT Level by Elevated CO_2 Treatment
Plants were grown under ambient CO_2 (40 Pa) or elevated CO_2 conditions (100 and 300 Pa). Total dry weight was determined at 40 days after seeding. Data represent means ± SD of four to five biological replicates. Different letters indicate significant difference ($P < 0.05$) determined by Tukey's test.

Figure 6. Number of Sulfate Ion Bound to Catalytic Site of Rubisco and the Structure Around the Solvent Channel Were Different between WT-Rubisco and CSS-Rubisco
(A) Structures of two RbcL and two RbcS of WT-Rubisco and CSS-Rubisco. The top left figure shows the whole WT-Rubisco structure comprising eight OsRbcL and eight OsRbcS. OsRbcL are colored green (chain A) and cyan (chain B), and OsRbcS and SbRbcS are colored yellow and orange, respectively. Sulfate ions are drawn in space-filling mode with oxygen and sulfur atoms colored in red and yellow, respectively.
(B) The structure of region 47-49 of WT-Rubisco and CSS-Rubisco. The left figure shows the structure of whole WT-Rubisco that is rotated 90˚ around the x-axis from the top left figure in (A). In this figure, residues 47-49 are colored red, and the residue form the inner wall of the entrance of the solvent channel (central pore). The right figure show the σA-weighted 2m*F*o-D*F*c electron density map contoured at 1.0σ. The map clearly shows alternative conformations of the main chain with E48 around region 48-49 in CSS-Rubisco. The CSS-Rubisco contains two different structures in this region. Amino acid numbering is based on spinach RbcS (Supplemental Figure 12).

Figure 7. Structural Comparison between WT-Rubisco and CSS-Rubisco Shows a Substantial Structural Difference in the βC-βD Hairpin

(A, B) Zoomed-in view of the catalytic site extracted from the boxed (red) area in Figure 6A. The structures of the catalytic site are shown with two sulfate ion (A) or 2CABP (B) in WT-Rubisco. Disordered regions are indicated by dots. Structural elements, residues, and ions are labelled.
(C) Superimposition of the βC-βD hairpin of sulfate-bound Rubisco (yellow and cyan) and 2CABP-bound Rubisco (red), extracted from the boxed area in A and B. The structural changes in the side chains of L74, F104, I102 and the βC-βD are shown as black arrow.
(D) Alignment of RbcS amino acid sequence around βC in sorghum, rice, and spinach.
(E, F) Space-filling representation around the βC-βD. The three residues (I/L102, F104, and L74) of WT-Rubisco (E) and CSS-Rubisco (F) are shown.

REFERENCES

Adams, P.D., Afonine, P.V., Bunkoczi, G., Chen, V.B., Davis, I.W., Echols, N., Headd, J.J., Hung, L.W., Kapral, G.J., Grosse-Kunstleve, R.W., et al. (2010). PHENIX: a comprehensive Python-based system for macromolecular structure solution. Acta Crystallogr. Sect. D Biol. Crystallogr. **66**: 213-221.

Aigner, H., Wilson, R.H., Bracher, A., Calisse, L., Bhat, J.Y., Hartl, F.U., and Hayer-Hartl, M. (2017) Plant RuBisCo assembly in *E. coli* with five chloroplast chaperones including BSD2. Science **358**: 1272-1278.

Andersson, I., and Backlund, A. (2008) Structure and function of Rubisco. Plant Physiol. Biochem. **46**: 275-291.

Andralojc, P.J., Elizabete Carmo-Silva, E., Degen, G.E., and Parry, M.A.J. (2018) Increasing metabolic potential: C-fixation. Essays Biochem. **62**: 109-118.

Anonymous (1994). The CCP4 suite: programs for protein crystallography. Acta Crystallogr. Sect. D Biol. Crystallogr. **50**: 760-763.

Bradford, M.M. (1976). A rapid and sensitive method for the quantitation of microgram quantities of protein utilizing the principle of protein-dye binding. Anal. Biochem. **72**: 248-254.

Bracher, A., Whitney, S.M., Hartl, F.U., and Hayer-Hart, M. (2017) Biogenesis and Metabolic Maintenance of Rubisco. Annu. Rev. Plant Biol. **68**: 29-60.

Chen, V.B., Arendall, W.B., 3rd, Headd, J.J., Keedy, D.A., Immormino, R.M., Kapral, G.J., Murray, L.W., Richardson, J.S., and Richardson, D.C. (2010). MolProbity: all-atom structure validation for macromolecular crystallography. Acta Crystallogr. Sect. D Biol. Crystallogr. **66**: 12-21.

Duff, A.P., Andrews, T.J., and Curmi, P.M. (2000). The transition between the open and closed states of rubisco is triggered by the inter-phosphate distance of the bound bisphosphate. J. Mol. Biol. **298**: 903-916.

Emsley, P., and Cowtan, K. (2004). Coot: model-building tools for molecular graphics. Acta Crystallogr. Sect. D Biol. Crystallogr. **60**: 2126-2132.

Esquivel, M.G., Genkov, T., Nogueira, A.S., Salvucci, M.E., and Spreitzer, R.J. (2013). Substitutions at the opening of the Rubisco central solvent channel affect holoenzyme stability and CO_2/O_2 specificity but not activation by Rubisco activase. Photosynth. Res. **118**: 209-218.

Evans, J.R. (1989). Photosynthesis and nitrogen relationships in leaves of C_3 plants. Oecologia **78**: 9-19.

Fernie, A.R., and Bauwe, H. (2020). Wasteful, essential, evolutionary stepping stone? The multiple personalities of the photorespiratory pathway. Plant J. **102**: 666-677.

Galmés, J., Kapralov, M.V., Andralojc, P.J., Conesa, M.A., Keys, A.J., Parry, M.A.J. and Flexas, J. (2014) Expanding knowledge of the Rubisco kinetics variability in plant species: environmental and evolutionary trends. Plant Cell Environ. **37**: 1989-2001.

Galmés, J., Capó-Bauçà, S., Niinemets, Ü., and Iñiguez, C. (2019). Potential improvement of photosynthetic CO_2 assimilation in crops by exploiting the natural variation in the temperature response of Rubisco catalytic traits. Curr Opin Plant Biol. **49**: 60-67.

Genkov, T., Meyer, M., Griffiths, H., and Spreitzer, R.J. (2010). Functional hybrid rubisco enzymes with plant small subunits and algal large subunits: engineered rbcS cDNA for expression in Chlamydomonas. J. Biol. Chem. **285**: 19833-19841.

Ghannoum, O., Evans, J.R., Chow, W.S., Andrews, T.J., Conroy, J.P., and von Caemmerer, S. (2005). Faster Rubisco is the key to superior nitrogen-use efficiency in NADP-malic enzyme relative to NAD-malic enzyme C_4 grasses. Plant Physiol. **137**: 638-650.

Hermida-Carrera, C., Kapralov, M.V., and Galmés J. (2016). Rubisco catalytic properties and temperature response in crops. Plant Physiol. **171**: 2549-2561.

Ishikawa, C., Hatanaka, T., Misoo, S., and Fukayama, H. (2009). Screening of high kcat Rubisco among Poaceae for improvement of photosynthetic CO_2 assimilation in rice. Plant Prod. Sci. **12**: 345-350.

Ishikawa, C., Hatanaka, T., Misoo, S., Miyake, C., and Fukayama, H. (2011). Functional incorporation of sorghum small subunit increases the catalytic turnover rate of Rubisco in transgenic rice. Plant Physiol. **156**: 1603-1611.

Kabsch, W. (2010). Xds. Acta Crystallogr. Sect. D Biol. Crystallogr. **66**: 125-132

Kabsch, W., and Sander, C. (1983). Dictionary of protein secondary structure: pattern recognition of hydrogen-bonded and geometrical features. Biopolymers **22**: 2577-2637.

Karkehabadi, S., Peddi, S.R., Anwaruzzaman, M., Taylor, T.C., Cederlund, A., Genkov, T., Andersson, I., and Spreitzer, R.J. (2005). Chimeric small subunits influence catalysis without causing global conformational changes in the crystal structure of ribulose-1,5-bisphosphate carboxylase/oxygenase. Biochemistry **44**: 9851-9861.

Laisk, A., and Loreto, F. (1996). Determining photosynthetic parameters from leaf CO_2 exchange and chlorophyll fluorescence (ribulose-1,5-bisphosphate carboxylase/oxygenase specificity factor, dark respiration in the light, excitation distribution between photosystems, alternative electron transport rate, and mesophyll diffusion resistance. Plant Physiol. **110**: 903-912.

Laterre, R., Pottier, M., Remacle, C., and Boutry, M. (2017). Photosynthetic trichomes contain a specific Rubisco with a modified pH-dependent activity. Plant Physiol. **173**: 2110-2120.

Lei, Y., Lu, L., Liu, H.Y., Li, S., Xing, F., and Chen, L.L. (2014). CRISPR-P: a web tool for synthetic single-guide RNA design of CRISPR-system in plants. Mol. Plant **7**: 1494-1496.

Lin, M.T., Occhialini, A., Andralojc, P.J., Parry, M.A., and Hanson, M.R. (2014). A faster Rubisco with potential to increase photosynthesis in crops. Nature **513**: 547-550.

Lin M.T., Stone, W.D., Chaudhari, V., and Hanson, M.R. (2020). Enzyme kinetics of tobacco Rubisco expressed in *Escherichia coli* varies depending on the small subunit composition. bioRxiv preprint doi: https://doi.org/10.1101/562223.

Long, S.P., Zhu, X.G., Naidu, S.L., and Ort, D.R. (2006) Can improvement in photosynthesis increase crop yields? Plant Cell Environ. **29**: 315-330.

Makino, A., Sakashita, H., Hidema, J., Mae, T., Ojima, K., and Osmond, B. (1992). Distinctive responses of ribulose-1,5-bisphosphate carboxylase and carbonic anhydrase in wheat leaves to nitrogen nutrition and their possible relationships to CO_2-transfer resistance. Plant Physiol. **100**: 1737-1743.

Makino, A., Shimada, T., Takumi, S., Kaneko, K., Matsuoka, M., Shimamoto, K., Nakano, H., Miyao-Tokutomi, M., Mae, T., and Yamamoto, N. (1997). Does decrease in

ribulose-1,5-bisphosphate carboxylase by antisense RbcS lead to a higher N-use efficiency of photosynthesis under conditions of saturating CO_2 and light in rice plants? Plant Physiol. **114**: 483-491.

Makino, A., Nakano, H., Mae, T., Shimada, T., and Yamamoto, N. (2000) Photosynthesis, plant growth and N allocation in transgenic rice plants with decreased Rubisco under CO_2 enrichment. J Exp Bot. **51**: 383-389.

Martin-Avila, E., Lim, Y.-L., Birch, R., Dirk, L.M.A., Buck, S., Rhodes, T., Sharwood, R., Kapralov, M.V., Whitney, S.M. (2020) Modifying plant photosynthesis and growth via simultaneous chloroplast transformation of Rubisco large and small subunits. Plant Cell Advance Access published July, 2020, doi:10.1105/tpc.20.00288

Matsumura, H., Mizohata, E., Ishida, H., Kogami, A., Ueno, T., Makino, A., Inoue, T., Yokota, A., Mae, T., and Kai, Y. (2012). Crystal structure of rice Rubisco and implications for activation induced by positive effectors NADPH and 6-phosphogluconate. J. Mol. Biol. **422**: 75-86.

Matt, P., Krapp, A., Haake, V., Mock, H.P., and Stitt, M. (2002). Decreased Rubisco activity leads to dramatic changes of nitrate metabolism, amino acid metabolism and the levels of phenylpropanoids and nicotine in tobacco antisense RBCS transformants. Plant J. **30**: 663-677.

Mikami, M., Toki, S., and Endo, M. (2015). Comparison of CRISPR/Cas9 expression constructs for efficient targeted mutagenesis in rice. Plant Mol. Biol. **88**: 561-572.

Morita, K., Hatanaka, T., Misoo, S., and Fukayama, H. (2014). Unusual small subunit that is not expressed in photosynthetic cells alters the catalytic properties of rubisco in rice. Plant Physiol. **164**: 69-79.

Murshudov, G.N., Skubak, P., Lebedev, A.A., Pannu, N.S., Steiner, R.A., Nicholls, R.A., Winn, M.D., Long, F., and Vagin, A.A. (2011). REFMAC5 for the refinement of macromolecular crystal structures. Acta Crystallogr. Sect. D Biol. Crystallogr. **67**: 355-367.

Peterhansel, C., and Offermann, S. (2012). Re-engineering of carbon fixation in plants - challenges for plant biotechnology to improve yields in a high-CO_2 world. Curr. Opin. Biotechnol. **23**: 204-208.

Porra, R.J., Thompson, W.A., and Kriedemann, P.E. (1989). Determination of accurate extinction coefficients and simultaneous equations for assaying chlorophylls a and b extracted with four different solvents: verification of the concentration of chlorophyll standards by atomic absorption spectroscopy. Biochim. Biophys. Acta **975**: 384-394.

Portis, A.R. Jr., Li, C., Wang, D., and Salvucci, M.E. (2008). Regulation of Rubisco activase and its interaction with Rubisco. J. Exp. Bot. **59**: 1597-1604.

Quick, W.P., Schurr, U., Scheibe, R., Schulze, E.-D., Rodermel, S.R., Bogorad, L., and Stitt, M. (1991) Decreased ribulose-l,5-bisphosphate carboxylase-oxygenase in transgenic tobacco transformed with "antisense" rbcS. I. Impact on photosynthesis in ambient growth conditions. Planta **183**: 542-554.

Sage, R.F. (2002). Variation in the kcat of Rubisco in C_3 and C_4 plants and some implications for photosynthetic performance at high and low temperature. J. Exp. Bot. **53**: 609-620.

Sage, R.F., Christin, P.A., and Edwards, E.J. (2011). The C_4 plant lineages of planet Earth. J. Exp. Bot. **62**: 3155-3169.

Salesse-Smith, C.E., Sharwood, R.E., Busch, F.A., Kromdijk, J., Bardal, V., and Stern, D.B. (2018). Overexpression of Rubisco subunits with RAF1 increases Rubisco content in maize. Nature Plants, **4**: 802-810.

Seemann, J.R., Badger, M.R., and Berry, J.A. (1984). Variations in the specific activity of ribulose-1,5-bisphosphate carboxylase between species utilizing differing photosynthetic pathways. Plant Physiol. **74**: 791-794.

Sharwood, R.E. (2017). Engineering chloroplasts to improve Rubisco catalysis: prospects for translating improvements into food and fiber crops. New Phytol. **213**: 494-510.

Sharwood, R.E., Ghannoum, O., and Whitney, S.M. (2016). Prospects for improving CO_2 fixation in C3-crops through understanding C4-Rubisco biogenesis and catalytic diversity. Curr. Opin. Plant Biol. **31**: 135-142.

Spreitzer, R.J. (2003). Role of the small subunit in ribulose-1,5-bisphosphate carboxylase/oxygenase. Arch. Biochem. Biophys. **414**: 141-149.

Spreitzer, R.J., Esquivel, M.G., Du, Y.-C., and McLaughlin P.D. (2001) Alanine-Scanning Mutagenesis of the Small-Subunit βA−βB Loop of Chloroplast Ribulose-1,5-Bisphosphate Carboxylase/Oxygenase: Substitution at Arg-71 Affects Thermal Stability and CO_2/O_2 Specificity. Biochemistry **40**: 5615-5621.

Tcherkez, G.G., Farquhar, G.D., and Andrews, T.J. (2006). Despite slow catalysis and confused substrate specificity, all ribulose bisphosphate carboxylases may be nearly perfectly optimized. Proc. Natl. Acad. Sci. USA **103**: 7246-7251.

Whitney, S.M., Sharwood, R.E., Orr, D., White, S.J., Alonso, H., and Galmes, J. (2011). Isoleucine 309 acts as a C_4 catalytic switch that increases ribulose-1,5-bisphosphate carboxylase/oxygenase (rubisco) carboxylation rate in Flaveria. Proc. Natl. Acad. Sci. USA **108**: 14688-14693.

Whitney, S.M., Birch, R., Kelso, C., Beck, J.L., and Kapralov, M.V. (2015). Improving recombinant Rubisco biogenesis, plant photosynthesis and growth by coexpressing its ancillary RAF1 chaperone. Proc. Natl. Acad. Sci. USA **112**: 3564-3569.

Willis, R.B., Montgomery, M.E., and Allen, P.R. (1989). Improved method for manual, colorimetric determination of total Kjeldahl nitrogen using salicylate. J. Agric. Food Chem. **44**: 1804-1807.

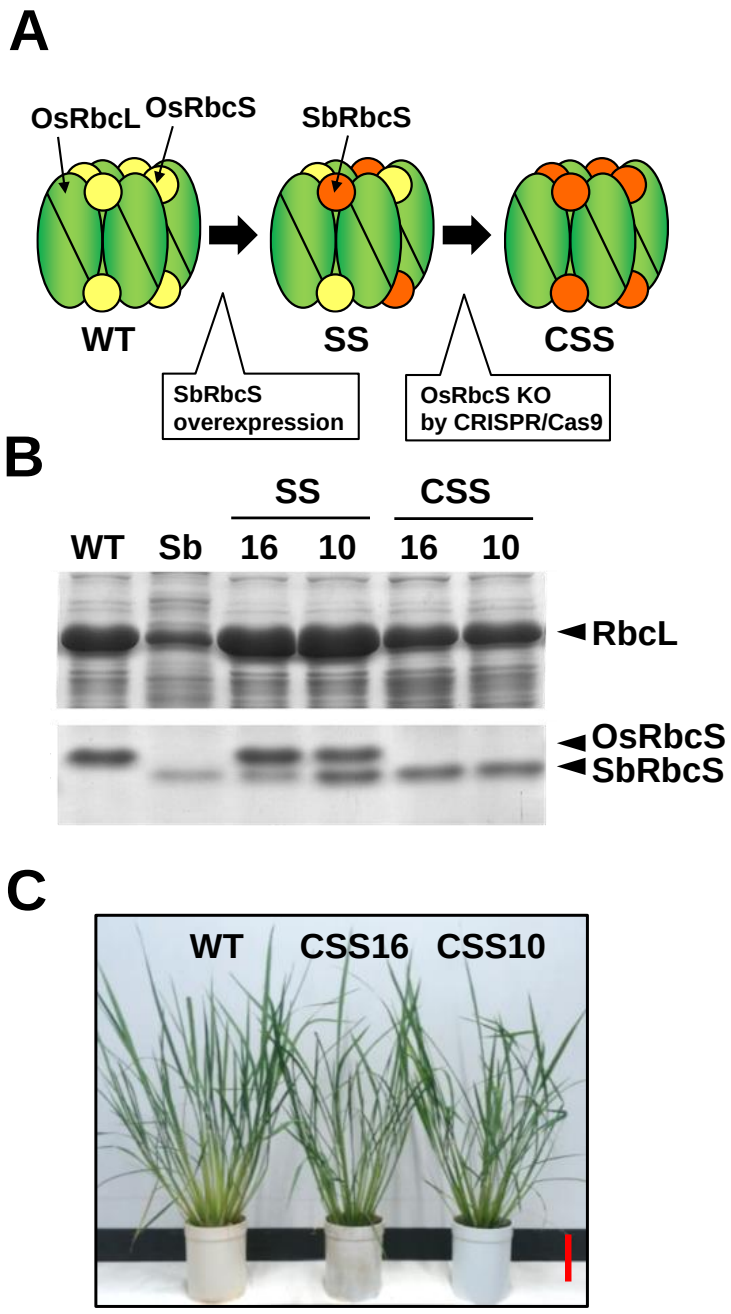
A
OsRbcL
OsRbcS
SbRbcS
WT
SS
CSS
SbRbcS overexpression
OsRbcS KO by CRISPR/Cas9
B
SS
CSS
WT
Sb
16
10
16
10
RbcL
OsRbcS
SbRbcS
C
WT
CSS16
CSS10

Figure 1

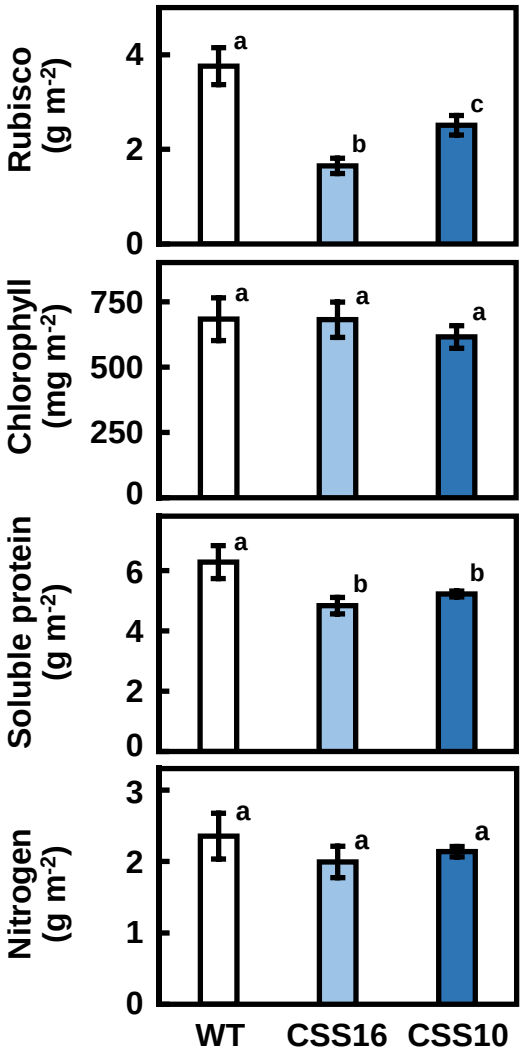
Rubisco (g m-2)
4
2
0
a
b
c
Chlorophyll (mg m-2)
750
500
250
0
a
a
a
Soluble protein (g m-2)
6
4
2
0
a
b
b
Nitrogen (g m-2)
3
2
1
0
a
a
a
WT
CSS16
CSS10

Figure 2

A

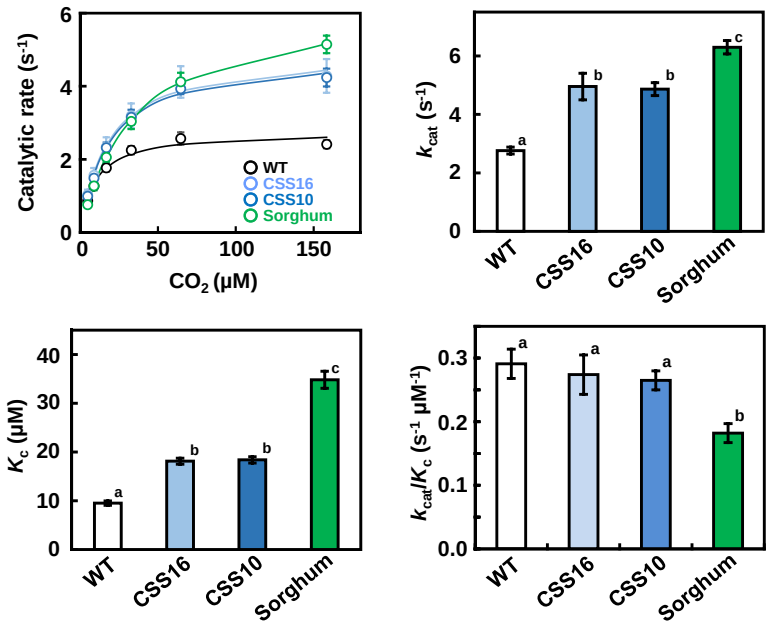

B

Line	k_{cat} (s^{-1})	K_c (μM)	K_c^{air} (μM)	K_m (RuBP) (μM)	$S_{c/o}$ (mol mol^{-1})	k_{cat}/K_c ($s^{-1}\mu M^{-1}$)	k_{cat}/K_c^{air} ($s^{-1}\mu M^{-1}$)
WT	2.76 ± 0.12 a	9.5 ± 0.5 a	13.8 ± 0.5 a	43.4 ± 2.7 a	94.0 ± 6.9 a	0.291 ± 0.023 a	0.200
CSS16	4.95 ± 0.45 b	18.1 ± 0.7 b	28.6 ± 0.8 b	39.7 ± 3.4 a	80.5 ± 5.6 b	0.274 ± 0.031 a	0.173
CSS10	4.87 ± 0.22 b	18.4 ± 0.7 b	28.5 ± 0.6 b	44.0 ± 5.2 a	78.1 ± 4.1 b	0.265 ± 0.015 a	0.171
Sorghum	6.30 ± 0.23 c	34.8 ± 1.8 c	41.2 ± 2.0 c	nd	nd	0.182 ± 0.015 b	0.153

Figure 3

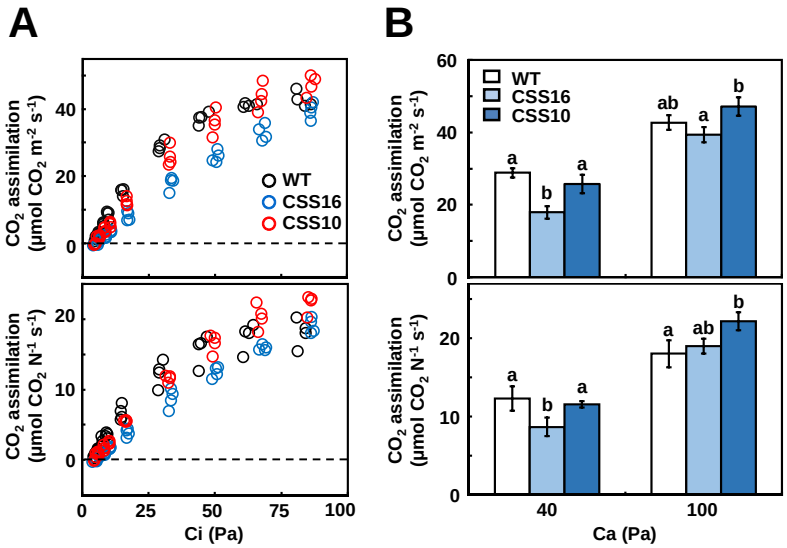
A
B
CO2 assimilation (µmol CO2 m-2 s-1)
CO2 assimilation (µmol CO2 N-1 s-1)
WT
CSS16
CSS10
Ci (Pa)
Ca (Pa)
a
b
a
ab
a
b

Figure 4

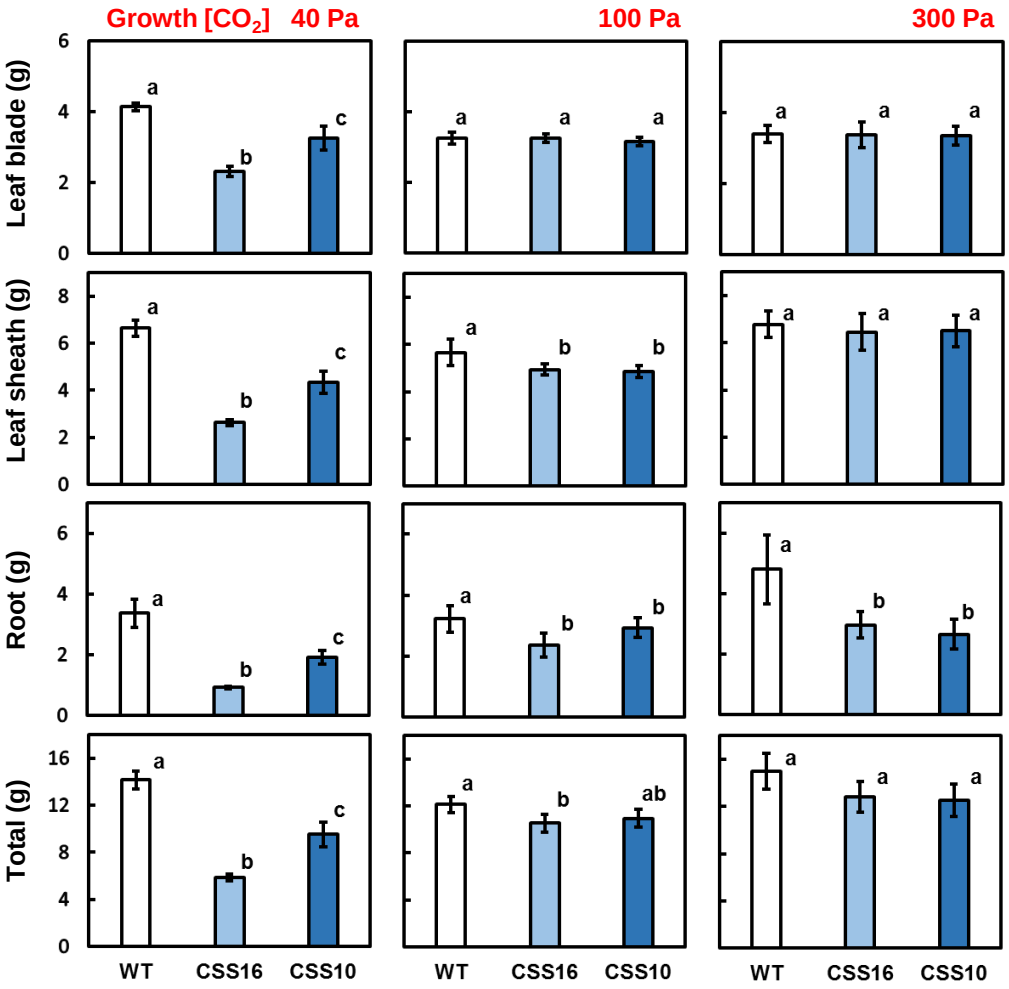
Growth [CO2] 40 Pa
100 Pa
300 Pa
Leaf blade (g)
Leaf sheath (g)
Root (g)
Total (g)
WT
CSS16
CSS10

Figure 5

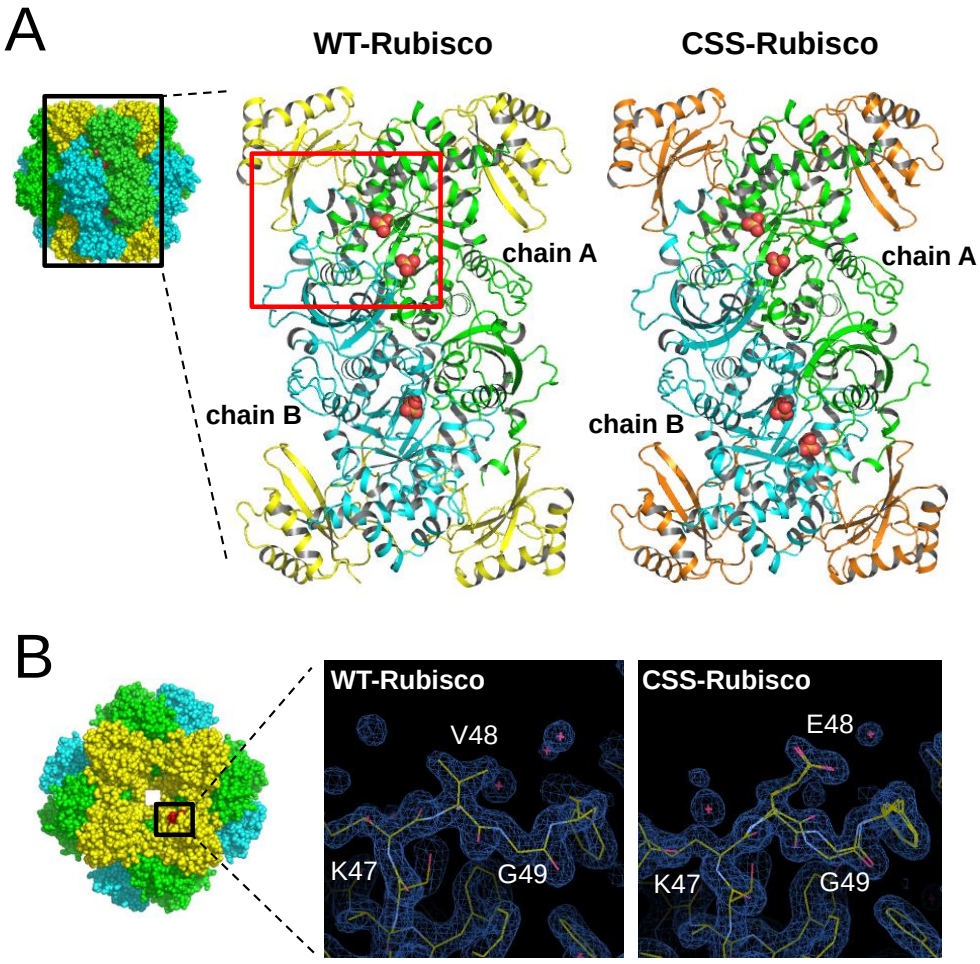
A
WT-Rubisco
CSS-Rubisco
chain A
chain B
chain A
chain B
B
WT-Rubisco
V48
K47
G49
CSS-Rubisco
E48
K47
G49

Figure 6

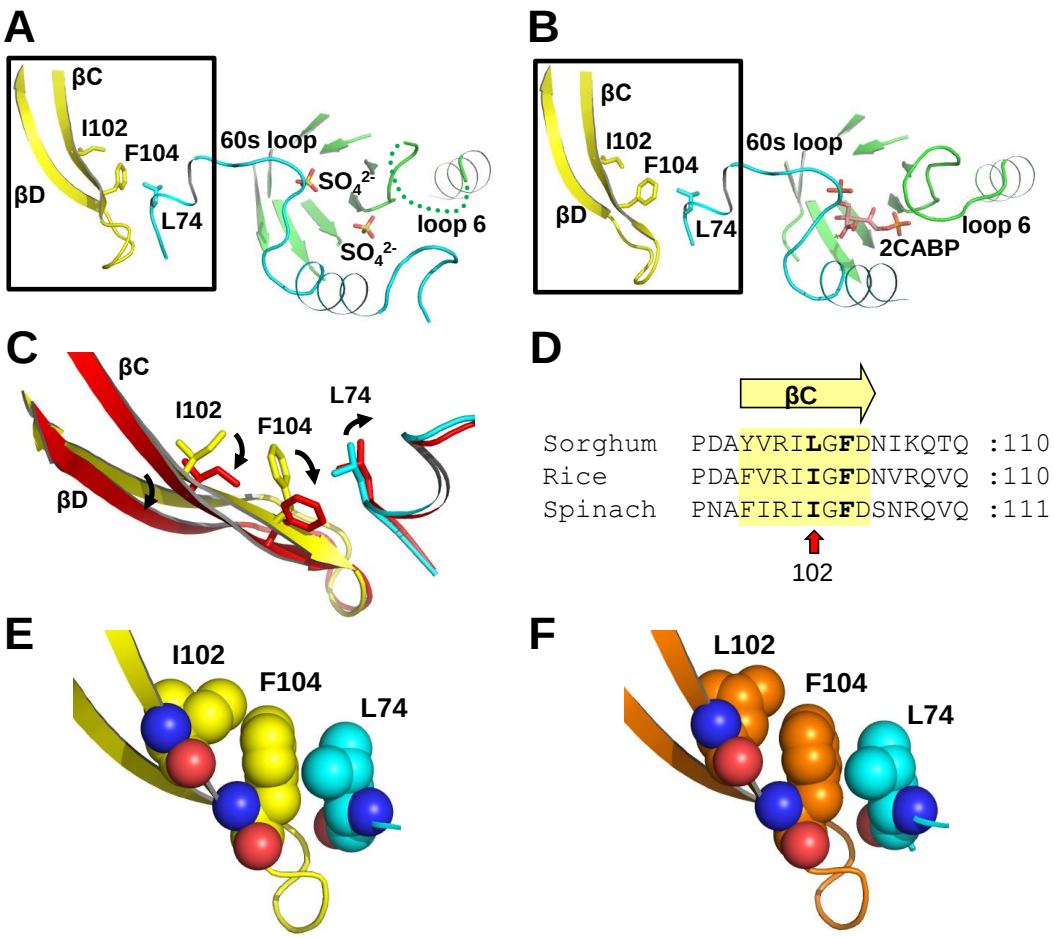
A
βC
I102
F104
βD
L74
60s loop
SO_4^{2-}
loop 6
SO_4^{2-}
B
βC
I102
F104
βD
L74
60s loop
loop 6
2CABP
C
βC
I102
F104
L74
βD
D
βC
Sorghum PDAYVRILGFDNIKQTQ :110
Rice PDAFVRIIGFDNVRQVQ :110
Spinach PNAFIRIIGFDSNRQVQ :111
102
E
I102
F104
L74
F
L102
F104
L74

Figure 7